

**Capturing the influence of groundwater dynamics on land surface processes using an
integrated, distributed watershed model**

Stefan J. Kollet and Reed M. Maxwell

*Atmospheric, Earth, and Energy Department, Lawrence Livermore National Laboratory,
Livermore, California*

Abstract

The influence of groundwater dynamics on the energy balance at the land surface is studied using an integrated, distributed watershed modeling platform. This model includes the mass and energy balance at the land surface; variably-saturated subsurface flow; explicit representation of the water table; and overland flow. The platform is suitable for large-scale, high-resolution simulations, because it is parallel, has a robust linear and non-linear solver and is designed for high performance computing. The model is applied to the Little Washita watershed in Central Oklahoma, USA and compared to runoff, soil moisture and energy flux observations. The connection between groundwater dynamics and the land surface energy balance is studied using a variety of conventional and spatial statistical measures. For a number of energy variables a strong interconnection is demonstrated with water table depth. This connection varies seasonally and spatially depending on the spatial composition of water table depth. For this particular watershed a critical water table depth range is established between 1 and 5m in which the land surface energy budget is most sensitive to groundwater storage. Finally, concrete recommendations are put forth to characterize this interconnection in the field.

1. Introduction and Motivation

Land surface processes are important as they control the transfer of water and energy between the lower atmosphere and subsurface. Characterization of these control mechanisms (e.g. evapotranspiration, ET, and recharge) is critical to the understanding and quantification of feedbacks between the atmospheric boundary layer, the land surface and the subsurface. This has been the subject of research for some time, both in the atmospheric community [1996; *Chen and Hu, 2004*] and the groundwater community [*NRC, 2004; Sophocleous and Perkins, 2000; Sophocleous, et al., 1999*]. The extent to which atmospheric and land surface processes are influenced by groundwater dynamics has been discussed previously [*Liang, et al., 2003; Maxwell and Miller, 2005; Quinn, et al., 1995; Yeh and Eltahir, 2005; York, et al., 2002*] though many aspects are still unresolved.

Groundwater dynamics and storage influences surface soil moisture and surface water flow. As there has been recent evidence that shallow soil moisture has a pronounced affect on atmospheric processes and weather prediction [*Chow, et al., 2006; Holt, et al., 2006; Patton, et al., 2005*] groundwater may be an important part of this feedback. In this paper, we present a methodology to characterize and evaluate the effect of groundwater on land surface processes (such as surface soil temperature and ET) and shallow soil moisture. We propose that there is more influence of the groundwater on land surface processes than previously thought and that zones of varying influence may be delineated within a watershed. In addition to this general methodology, numerical simulations in conjunction with statistical [e.g., *Grayson, et al., 2002*] analysis will be presented to quantify these effects.

Originally developed as a lower boundary condition for global climate models [*Manabe, et al., 1970*], land surface models (LSMs) have steadily evolved and become more sophisticated

(see e.g. the review by [Betts, et al., 1996]). A large number of LSMs have been developed, with differing parameterizations [Chen, et al., 1997; Dai, et al., 2003; Henderson-Sellers and Henderson-Sellers, 1995; Lohmann, et al., 1998; Pitman, et al., 1999; Qu, et al., 1998; Schlosser, et al., 2000; Shao and Henderson-Sellers, 1996]. Until recently, LSMs have ignored the saturated zone (i.e. groundwater); though there has been recent work incorporating a groundwater component into LSMs [Liang, et al., 2003; Maxwell and Miller, 2005; Yeh and Eltahir, 2005]. Studies by Liang et al. [2003] and Yeh and Eltahir [2005] incorporated groundwater processes into a land surface model and demonstrated feedbacks. Maxwell and Miller [2005] explicitly coupled a saturated-unsaturated groundwater model to a land surface model and show feedbacks from the water table dynamics, particularly in shallow soil moisture. While these studies suggest an interconnection of groundwater dynamics and the energy balance at the land surface they have not accounted for three-dimensional subsurface flow and overland flow, nor has a study clearly demonstrated correlation between water table dynamics and surface processes on the watershed scale.

In this paper, a numerical approach that realizes a fully-three dimensional, coupled land-surface, overland flow and subsurface model is presented. Using simulations of a watershed in Central Oklahoma, USA, statistical tools are employed to establish the connection between groundwater and land surface processes and to delineate zones of spatial correlation.

2. Conceptual Approach

The underlying hypothesis in this work is that there exists a linkage between groundwater dynamics and the mass and energy balance at the land surface. This linkage occurs via the shallow soil moisture, which is directly impacted by processes at the land surface, such as ET,

and the location of the water table. The question arises when does the groundwater table exert control on the distribution of shallow soil moisture? Three different cases can be identified that are illustrated in Figure 1: (1) the depth to the water table, D , is small ($D < 10^0$ m); (2) the water table is at intermediate depth ($D \sim 10^0$ m); and (3) the water table is far from the land surface ($D > 10^0$ m).

In Case 1, processes at the land surface are not water limited and do not depend on small variations in the water table depth, i.e. the linkage between the groundwater dynamics and land surface processes can be weak. In Case 3, processes at the land surface are strongly water limited and again do not depend on small variations in the water table depth. Water transport is directed downward in case of recharge and there is no significant upward redistribution of soil moisture. Case 1 and Case 3 constitute two different end members in the functional relationship between groundwater dynamics and the energy balance.

In Case 2, the water table is at, what we define as, the critical depth from the ground surface. Small changes in D cause significant vertical redistribution of soil moisture near the land surface resulting in changes of the mass and energy balance at the land surface. Since the energy and mass balance is expected to be continuous for finite D values, Case 2 characterizes the transition between Case 1 and Case 3.

The above conceptual model is based primarily on vertical moisture distribution in a single soil column. Figure 2 expands on this concept, depicting an idealized hillslope transect with a stream on the left. This transect has been divided into region A) with shallow depth to groundwater; B) with an intermediate depth to groundwater; and C) with a large depth to groundwater. These three regions can be associated conceptually with the three soil columns in Figure 1 and are hydraulically connected via topographically driven groundwater flow.

In the case of topographically driven groundwater flow, the water table closely follows the topography, i.e. topographic lows coincide with groundwater discharge areas, whereas topographic highs coincide with recharge areas. Thus, the water table depth increases from the valleys to the hill tops. We then expect to find case 1 and case 2 in the valleys and at the hilltops, respectively, and case 3 in a transition zone along the hillslope extending from the valleys toward the hilltops. This conceptual approach is a simplification of real-world systems. For example, subsurface heterogeneity in the hydraulic properties, on a number of spatial scales, may result in a non-uniform moisture distribution and perched water lenses, which may influence the water and energy balance at the land surface. However, we believe that on intermediate to large spatial scales, our model provides insight into fundamental processes related to the linkage of the mass and energy balance at the land surface. This is similar to Toth's classical analysis of watershed hydrodynamics using a simple analytical solution [Toth, 1963]. Here a more realistic system is studied, using numerical simulations, relaxing many of the simplifying assumptions in Toth's approach.

The conceptual model put forth above linking groundwater dynamics and the energy balance at the land surface is only one and two dimensional (i.e. a single-column representation of the linked surface-subsurface domain). Groundwater dynamics may have transient, three-dimensional components, i.e. perturbations of the hydraulic potential in one location propagate through the system at a certain speed, which is mainly determined by the hydraulic diffusivity of the aquifer. Thus, an increase in the water table at one location due to e.g. recharge from a rain storm will cause a response throughout the entire system. These are well known principles of groundwater dynamics that have been reviewed recently by [Alley, *et al.*, 2002]. Therefore, changes in groundwater levels in recharge areas along ridges and hilltops will influence

groundwater behavior in discharge areas along streams and seeps directly affecting the energy balance at these locations. This type of linkage is determined by the interrelationship of our 1D groundwater-energy linkage with 3D hydrodynamic effects on the watershed scale.

3. Coupled model approach

ParFlow is a variably saturated groundwater flow model with an integrated overland flow simulation capability. It solves the three-dimensional Richards equation using cell-centered finite differences in space and an implicit backward Euler scheme in time. ParFlow was designed for high performance computing applications and is, thus, parallel. It lends itself to large scale high resolution simulations that require the efficient use of large computational resources. To simulate fully-coupled surface-subsurface flow, a free-surface overland flow boundary condition is applied at the land surface and consists of the kinematic wave equation. This equation is discretized using a finite control volume approach in space and also an implicit backward Euler scheme in time. The coupled equations are solved simultaneously using a Newton-Krylov method with multigrid preconditioning. An additional advantage of ParFlow is the use of an advanced octree data structure for the rendering of overlapping objects in 3D space, which facilitates geologic modeling of the subsurface and the representation of the topography using information from digital elevation models and watershed boundaries. For details the reader is referred to *Ashby and Falgout [1996]*, *Jones and Woodward [2001]*, and *Kollet and Maxwell [2006]*.

For this work, ParFlow has been extended to incorporate physical processes related to the energy and mass balance at the land surface. This was accomplished by integrating a land surface model, the Common Land Model (CLM, [*Dai, et al., 2003*]), into ParFlow building on the

approach by *Maxwell and Miller* [2005]. In their approach, ParFlow replaced the soil moisture module of CLM by replacing the soil column/root zone formulation and providing CLM with the moisture distribution at each time step. In turn CLM, provided ParFlow with the fluxes at the land surface, such as evapotranspiration and infiltration from precipitation. The passing of information between both models was performed via input and output files of each model. Additionally the coupled model was run in single column mode in undistributed fashion.

In the study presented here, ParFlow still replaces the soil column/root-zone formulation in CLM [*Maxwell and Miller, 2005*] and CLM calculates the mass and energy balance at the land surface. Furthermore, CLM was incorporated into ParFlow in distributed manner as a module, i.e at each x,y location in the computational domain, an individual CLM tile coincides with the upper face of an individual cell at the top of the subsurface model in ParFlow. An additional difference from *Maxwell and Miller* [2005] is the replacement of the TOPMODEL-based runoff scheme in CLM with the integrated overland flow simulator in ParFlow. In this coupled model, CLM is also parallel including a parallel input and output file structure. Atmospheric data, such as temperature, precipitation, solar radiation, humidity, and barometric pressure, are used to force the model and can be applied in a distributed fashion as well.

As aforementioned, ParFlow calculates the mass balance in the subsurface, while CLM calculates the mass and energy balance at the land surface [*Dai, et al., 2003* {*Maxwell, 2005* #107; *Maxwell and Miller, 2005*]. The latter include evaporation from canopy and the ground surface; transpiration from plants; ground heat flux; freeze-thaw processes and sensible heat fluxes. Since the governing equations have been discussed in the great detail in the literature, we will only briefly reiterate some fundamental equations to illustrate the intrinsic coupling of the mass and energy balance.

At the land surface, the mass and energy balance can be written as

$$R_n(\theta) = H(\theta) + LE(\theta) + G(\theta) \quad (1),$$

where R_n is net radiation, H is the sensible heat, LE is latent heat, G is ground heat flux, and θ is the soil moisture at the land surface. Hence, all energy variables depend on the water content at or close to the ground surface.

The mass balance of the subsurface can be written as follows

$$S_s \theta \frac{\partial \psi}{\partial t} + \frac{\partial \theta(\psi)}{\partial t} = \nabla \cdot q(T) + q_s(\theta) \quad (2),$$

where, S_s is the specific storage, ψ is the soil pressure head, q is the water flux, T is temperature, t is time, and q_s is a general source/sink term. At or near the land surface, q_s can be expressed as

$$q_s = LE(\theta) + q_g(\theta) \quad (3),$$

where q_g is the flux of water infiltrating at the land surface due to precipitation and canopy throughfall and/or surface runoff.

Equations (1) through (3) illustrate the coupling a of the subsurface-land surface system that occurs mainly through the nonlinear source q_s and the dependence of the energy variables on θ . The strength of coupling and the resulting non-linearity depends on the parameterization of the relationships $R_n(\theta)$, $H(\theta)$, $q_s(\theta)$, $G(\theta)$, $\theta(\psi)$, and $q(T)$ and the inherent assumptions and simplifications. Some simplifications applied in the coupled modeling approach include the independence of q on T (the hydraulic conductivity of the subsurface materials are independent of T); neglecting the convective component in G ; and neglecting explicit vapor transport in the subsurface in the calculation of ground evaporation.

A more detailed discussion of parameterization schemes of different components of the energy balance at the land surface will be given below. This will provide insight into the causes

of the influence of ground water dynamics on the mass and energy balance at the land surface as calculated by CLM.

4. Little Washita Watershed: Description and Model Setup

In the current work, the coupled ParFlow-CLM (PF.CLM) watershed model was applied to the Little Washita watershed, an approximately 600 square kilometer watershed located in the Southern Great Plains region of the United States in Southwestern Oklahoma (Figure 3). The Little Washita watershed lies within the DOE Atmospheric Radiation Monitoring (ARM) facility. The model inputs include spatially uniform atmospheric forcing, spatially distributed land and soil cover information, topography, and effective subsurface geologic model.

The PF.CLM watershed model was constructed with a lateral spatial discretization ($\Delta x = \Delta y$) of 1km and a vertical discretization (Δz) of 0.5m using 32x45x390 cells in the x, y and z dimension, respectively, resulting in a total of 561,600 rectilinear elements. The lower z -coordinate originates at 260m above mean sea level and the lower-left cell center latitude and longitude are 34.74 and -98.30, respectively. A preprocessed digital elevation model (DEM) was used to define the land surface boundary and thus the depth of the subsurface (defined as the topographic elevation to the bottom of the model), which ranged from a minimum of 63m to a maximum of 191m. The boundary conditions were no-flow along all sides of the model domain except at the land surface, where an overland flow boundary condition was prescribed. Note that the model domain extended beyond the watershed boundaries; therefore the location of the three-dimensional water divide of the Little Washita watershed developed naturally in the model.

The model used USGS information for the surface soil types (Figure 5). The vanGenuchten parameters required for the soil moisture pressure head relationships were

obtained from the RAWLS data base [Schaap and Leij, 1998]. The deeper subsurface was based on an effective representation using effective parameters values based on the analysis of public records of some 200 boreholes in the region. The properties of the effective subsurface are as follows: saturated hydraulic conductivity, $K_{sat}=4.8$ m/d, porosity, $\phi=0.4$, vanGenuchten parameters $\alpha=3.5$ (1/m) and $n=2$, and the residual saturation $S_{res}=0.2$.

USGS information was also used for the surface vegetation cover (Figure 5).

Corresponding vegetation parameters were obtained following the standard of the International Geosphere-Biosphere Program (IGBP).

In order to obtain a realistic initialization of all state variables the model was run repeatedly over one year using the same spatially uniform forcing until a dynamic equilibrium was reached (commonly referred to as model spinup). Starting at the beginning of the spinup the water table was initialized 2m below ground surface everywhere and the model was run over successive years until equilibrium was reached, which was seven years. In this study, spatially uniform forcing from the North American Regional Reanalysis (NARR) data set was used to eliminate atmospheric effects on the energy balance at the land surface from the analysis. The simulation period was from September 1998 until August 1999 using a time step size of one hour.

Figure 4 below shows an example soil moisture distribution in the Little Washita watershed in July after the spinup was completed. The non-uniform moisture distribution is a result of the topography and the non-uniform soil and land cover distributions, shown in Figure 5. Note, groundwater naturally converges and discharges in the valley, forming the Little Washita River.

5. Comparison to field data

The Little Washita watershed has been subject of many field campaigns in the ARM and SGP framework [e.g., *Jackson, et al.*, 1999]. These field campaigns focused on measurements of shallow soil moisture, soil temperature, and variables of the atmospheric boundary layer and have produced a number of unique datasets which are shown in Figure 3. Remote sensing data (both from satellites and aircraft over-flights) are also available, because many of the field campaigns were directed at the application of remote sensing for measuring of land surface variables. Additionally, there are data available from the following sources: 1) USGS stream gauging stations; 2) the Oklahoma Mesonet; 3) Ameriflux tower; 4) Soil Climate Analysis Network (SCAN); and 5) the ARS Micronet. Thus, there are data from the shallow subsurface upward.

Although there are a number of groundwater wells in the watershed, almost all are private and have only a single water-level measurement taken at the time of installation. Unfortunately, there is virtually no groundwater data available during the study period from September, 1998 until August, 1999 or any other time period that is also covered by the aforementioned data sources.

Nevertheless, the available observations can be used to demonstrate the fitness of the model to simulate the mass and energy balance in an integrated and distributed fashion on the watershed scale. Here we show a brief comparison of the simulated soil moisture with observations from the SCAN station, simulated energy fluxes with the observations from the Ameriflux tower, and simulated stream discharge with observations from a USGS stream gauging station. Note that the model was not calibrated to measured data as mentioned earlier. During the spinup process, the saturated hydraulic conductivity of the subsurface model was

adjusted slightly using limits established by effective theory to better match the measured hydrograph.

Comparison with the measured hydrograph from the USGS station 7327550 shows good agreement during baseflow conditions from September 1998 until the end of February 1999 (Figure 6). After February 1999, the model dries out too quickly. Additionally the model generally captures the timing of peak discharges quite well, though overestimates the peak flow rate. From July until September, the model is not able to capture the low flow conditions, but soil moisture values are maintained at or close to saturation in the river valley during that time period.

Figure 7 shows the comparison with the soil moisture data from the SCAN site at about 20 and 50 cm depths with averaged simulated values of the top model layer. The averaged simulated values were derived from equally weighted values of the four modeling cells closest to the SCAN site. Despite the fact that the comparison is based on a point measurement and simulation results that use 1km lateral resolution, the results agree well. The model is able to capture the major wetting and drying cycles. The peaks are generally underestimated from December 1998 until June 1999, whereas the model does not dry out quickly enough from June until August 1999. Reasons for these discrepancies might include spatial grid resolution, application of uniform atmospheric forcing, and the choice of effective subsurface and land surface parameters.

To evaluate the energy simulations we compared daily averaged estimates of latent heat (LE) from the model output to results from the Ameriflux tower in the domain (Figure 8). The model overestimates LE , particularly from September until December 1998, however the overall trend in LE is captured reasonably well. Other studies have shown the complexities and

difficulties of comparisons with Ameriflux tower data that are related with, for example, fetch uncertainty [Twine, *et al.*, 2000]. The large discrepancies especially in September 1998 may also stem from the spinup that assures that the energy balance at the end of August 1999 is the same as the energy balance at the beginning of September 1998. Yet, the energy balance at the end of August 1999 is not at all similar to the actual energy balance at the end of August 1998 that was recorded by the Ameriflux tower.

Although the comparison shows discrepancies between simulated and measured data, the model reproduces major trends and large parts of measured time series reasonably well. Significant improvement of model performance might be accomplished through a calibration exercise and parameter uncertainty study, which is outside the scope of the current work. Since the model is not used for prediction purposes, but for process identification and examination, we feel that the fitness of the model to capture major physical processes and behavior of the real system is adequate.

6. Model Results

6.a Yearly averaged, spatially distributed data

In this section, we present some yearly-averaged, summary results from the coupled model spinup mentioned in the previous section. Figure 9 shows plots of yearly averages of the components of the energy balance (from Equation 1), depth to groundwater level and ground surface temperature. These components are discussed below.

The depth to the water table (Figure 9b) correlates strongly with topography (Figure 9a), i.e. the water table is shallow in the valley and deep along the hilltops. Inspection of the different components of the energy balance shows the impact of vegetation cover and the shallow water

table (Figure 9e-f). The influence of the water table is especially pronounced for the ground heat flux (Figure 9h). While soil cover has surprisingly little influence on the average fluxes, vegetation cover is clearly a primary factor. Soil cover only plays a significant role in the distribution of the relative saturation (Figure 9c)

What cannot be deduced from this Figure, however, is the contribution that different vegetation types impart on the water and energy flux variables to assess the impact of groundwater dynamics, i.e. water table depth. A more detailed analysis is performed in the following sections using scatter plots and geostatistics.

6.b Scatter plots

In this section, we use scatter plots to analyze the interdependence between different components of the land surface mass and energy balance and water table depth (and thus groundwater dynamics). Figure 10 shows scatter plots of yearly averaged values of a) net radiation, R_n ; b) latent heat, LE ; c) sensible heat, H ; and d) ground heat flux, G as a function of yearly-averaged water table depth, D . In these plots, each symbol represents an individual x -, y -location in the computational domain with a corresponding yearly averaged energy and water table depth value. Because of the spatially varying vegetation, different symbols were used for grasslands, open shrublands, croplands, and deciduous forest to identify the vegetation cover at individual x - y -locations.

Preliminary inspection of the Figure 10 shows wide scatter that can be primarily attributed to the spatially varying vegetation types and secondarily to soil type. Well-defined relationships between D and the different components of the energy budget emerge for open shrublands, croplands, and deciduous forest.

These relationships are characterized by a segmented behavior including two flat segments separated by a steep segment of positive or negative slope in the range $1 < D < 5\text{m}$. The flat segments indicate no sensitivity of the energy variables to D and are formed by value pairs at locations with either relatively small or large D values, i.e. very shallow or deep water tables. The steep segments, which are particularly pronounced in the case of G (Figure 10d), form the range in which the energy variables are most sensitive to D . For radiation, R_n , latent heat flux, LE , and ground heat flux, G the correlations with D are negative. Thus the energy fluxes decrease with increasing water table depth. For sensible heat flux, H , the correlation is positive. For grasslands, energy variables show generally very little dependence on D , except in the case of G . In the range $1 < D < 5\text{m}$, energy fluxes can vary by up to a factor of two in the case of H and the vegetation type deciduous forest.

6.c Spatial univariat and bivariat statistics

In order to test whether the model captures the spatial structure of the shallow soil temperature appropriately, we developed omni-directional, unit semivariograms using data from the ARS Micronet network (located in the Little Washita watershed as shown in Figure 3) for June, July and August 1999 and compared those with the predicted semivariograms from the simulations. The comparison is shown in Figure 11 and demonstrates good agreement between the measured and predicted spatial structure in the shallow soil temperature. In both cases, the semivariances stabilize after about 6km lag size. However, for small lag sizes there is only a limited amount of measured data and, naturally, more noise in the unit semivariograms.

In the model, the water table closely follows the topography. The water table exhibits a spatial structure that is influenced by the topography and characterized by relatively shallow

water levels in the topographic depressions and relatively deeper water levels along the hilltops (Figures 4 and 9). Because the water table follows the topography, variograms of simulated water table depths, D , can be used to identify the scale of the spatial structure of D that arises from topographically-driven processes. Figure 12 shows the directional, unit semivariograms in the x - and y - directions for the yearly averaged D values. These semivariograms show differences in structure in the two directions. In the x -direction, which is aligned with the principal flow direction of the Little Washita, the sill is reached for a lag size of about 11km. In the y -direction which is mainly transverse to the Little Washita, the spatial correlation in water table depth appears to deteriorate at a smaller lag size of about 7km.

In order to study the cross-dependence of the components of the energy balance and ground surface temperature T_s with water table depth, monthly cross correlograms were generated (Figure 13). The components of the energy balance are net radiation, R_n ; latent heat, LE ; sensible heat, H ; and the ground heat flux, G . Ground surface temperature was included in the analysis, because it contributes to the energy balance and is a commonly monitored variable in the field.

In Figure 13, the net radiation, R_n , does not show cross dependence with D over the entire year on all spatial scales. Latent heat, LE , shows weak negative cross dependence in December, January, and February. Sensible heat, H , shows weak positive cross dependence in July, August, and September. The largest cross dependence was observed for the ground heat flux, G , with maximum values of about 0.7 and -0.7 in January and July respectively. The cross correlation values are positive in the cool months of the year (November until March) and become negative in the warmer months from April until September. The transition from positive to negative values occurs quite abruptly from March to April. This is in contrast to the reverse case, when

the cross dependence changes more gradually from negative to positive values from September to October.

Cross correlations were also calculated for the ground surface temperature, T_s , which shows positive cross correlation from July until September and negative values for December and January. For lag sizes larger than 7km, the cross correlations for all variables are close to zero over the entire year. In cases of significant cross correlation, the scale of the cross correlation structure appears to be 6 to 7km. Thus, the scale of the cross correlation structure is comparable to the hillslope scale depicted in Figure 12.

Because strong cross dependence was observed for ground heat flux and water table depth, unit directional semivariograms in the x - and y -directions were calculated for each month of the year (Figure 14) The directional semivariograms for monthly-averaged water table depths show directional variation (Figure 14), which was also true for the semivariograms of the yearly averages in case of D (Figure 12). There is also very little variation in semivariograms from month to month.

In most months, the semivariograms of G also show a directional dependence. This dependence is very similar to the directional dependence of the semivariograms of D with smaller correlation lengths in the x - than in the y -direction. The overall shape of the semivariograms of G and D are also very similar over most of the year. However, there is a shift in the semivariograms of G toward slightly smaller correlation lengths that is especially apparent in January.

In March and April, and from August until October, the directional dependence weakens in the G semivariograms. In these months the semivariograms in the y -direction approach the semivariograms in the x -direction and it appears that the spatial structure in G becomes self-

governing, i.e. independent of D . The correlation length decreases to approximately 5km in the x - and y - direction. The disappearance of the directional dependence and apparent decoupling of the structure of G from D coincides with transition in the cross correlation from positive to negative values in March and April, and from negative to positive values from August until September (Figure 13).

7. Discussion of Results

7.a Scatter Plots

The scatter plots (Figure 10) illustrate the correlations of the components of the energy balance of the land surface with water table depth and, thus, groundwater dynamics. The three segments of the curves in Figure 10 are characterized by two flat segments for the ranges $0.001 < D < 1\text{m}$ and $D > 5\text{m}$ that are separated by a steep segment with positive or negative slope for the range $1 < D < 5\text{m}$. We explain this behavior as follows: in the range $0.001 < D < 1\text{m}$, the water table is very close to land surface and the system is never water limited. This is true even during the very dry months of the year, because moisture is easily redistributed vertically upward from the shallow water table. The shallow water table is maintained in the valleys by topographically driven flow. Thus the first segment corresponds to Case 1 in Figure 1 and Zone A in Figure 2 as discussed in Section 3.

In the range $D > 5\text{m}$, the water table is far enough below the root zone that the system is water limited. This is true in general, except during and shortly after precipitation events. In areas where $D > 5\text{m}$ (primarily on the hill tops), soil moisture is not distributed vertically upward from the water table toward the land surface; transport of moisture is solely downward. This range is equivalent to Case 3 in Figure 1 and Zone C in Figure 2 of Section 3.

In the range $1 < D < 5\text{m}$, both negative and positive correlations exist between the different energy variables and D . This range is equivalent to Case 2 as defined in Figure 1 and designates a critical water table depth for this system (as defined in Section 3) between 1 and 5m below the ground surface. The distinct correlations for different vegetation types and energy variables stem from the parameterizations of the different processes in the land surface model and from variably saturated groundwater flow above the water table. This will be discussed in detail by inspecting the physical components of latent heat, LE : ground evaporation and transpiration.

In CLM [Dai, *et al.*, 2003], ground evaporation, E_g is defined as a conductance or a resistance in the form

$$E_g = \rho_a \frac{(q_g - q_a)}{r_d} \quad (4),$$

where ρ_a is the intrinsic density of air; q_g is the air specific humidity at the ground surface; q_a is the air specific humidity at reference height z_q obtained from atmospheric forcing; and r_d is the aerodynamic resistance of evaporation between the atmosphere at z_q . In CLM, the specific humidity of the ground surface, q_g , is parameterized as

$$q_g = q_{sat} e^{\left(\frac{\psi g M}{RT}\right)} \quad (5),$$

where ψ is the soil total potential [L], g is the gravity constant [LT^{-2}], M is the molar weight of water [M]; R is the gas constant [$\text{JM}^{-1}\text{K}^{-1}$]; and T is the temperature at the ground surface [K].

The aerodynamic resistance, r_d , is based on the Monin-Obukhov similarity principle and is also a function of q_g . In general, evaporation from the ground decreases with decreasing q_g , which explains much of the negative correlation of LE and D in the range $1 < D < 5\text{m}$. Yet, LE includes transpiration, E_{tr} , which competes with E_g for the amount of available moisture (and thus energy) in the shallow subsurface. In CLM, E_{tr} is parameterized as follows

$$E_{tr} = \sigma_f L_{SAI} \delta(E_f^{pot}) L_d \frac{r_b}{r_b + r_s} \quad (6),$$

where σ_f is the vegetation fraction; L_{SAI} is the stem plus leaf area index; δ is the step function; E_f^{pot} is the potential evaporation from wet foliage; L_d is the dry fraction of foliage surface; r_b is the conductance of heat and vapor flux from leaves; and r_s is the stomatal resistance.

In Equation 6, r_s depends on $\psi(\theta)$ and increases with decreasing water content. This dependency is weak as transpiration may still occur even under very dry conditions. The result is small contribution of E_{tr} to the correlation between LE and D in the range $1 < D < 5$ m. Other LSMs use different stomatal resistance parameterizations [Qu, *et al.*, 1998, Table 1] and the correlation between LE and D is, of course, very sensitive to this parameterization..

For LE , the critical depth is between about 1 and 5m. Modifications in the parameterization schemes (e.g. a stronger dependence of E_{tr} on $\psi(\theta)$) would change the range of the critical depths at which water table effects are significant. However, the overall behavior, i.e. the segmentation of the curves for the different vegetation types, would not be affected. Thus, the underlying hypothesis that there exist some critical depths at which the water table cannot be neglected appears to be valid in general terms.

It is also expected that the critical depth depends on the soil type, because the parameters of the pressure-saturation relationship vary with soil type. In the PF.CLM model as applied to the Little Washita watershed, the upper layer contains the distributed pedology, while the rest of the subsurface is approximated as a uniform, effective continuum (Section 4). The scatter plot analysis (Figure 10) exposes that variation in soil type had little influence on the energy balance at the land surface. This is reflected by the small scatter of the data for each individual vegetation type. While the insensitivity of critical depth to soil type might seem counterintuitive, a more in-

depth analysis using LE shows the consistency of this result. Although, in the model, the parameterization of LE depends on $\psi(\theta)$, it is most sensitive to $\psi(\theta)$ when the soil is very dry, i.e. when E_g is reduced. For these $\psi(\theta)$ values θ is at or near the residual water content. This is true regardless of soil type and results in a homogenization of $\psi(\theta)$ and thus the energy fluxes. A more pronounced effect of the soil type would be expected at intermediate water contents, when the sensitivity of θ to ψ is largest. But in that $\psi(\theta)$ range, the sensitivity of the energy variables to soil moisture is relatively small. The ground evaporation-pressure, $E_g(\psi)$, functional relationship described by Equation 5 is shown in Figure 15. This Figure indicates that ground evaporation is most sensitive to ψ in the range $10^2 < |\psi| < 10^5$ m. The upper limit of this range ($|\psi| \approx 10^2$ m) coincides with the wilting point threshold used in the calculation of E_{tr} in CLM [Dai, et al., 2001]. For $|\psi| > 10^2 - 10^3$, the sensitivity of θ to changes in ψ is small also for structured soils, such as clay, and θ is rapidly approaching the residual water content. Thus the overlap of the sensitivity ranges of the energy variables and θ on $\psi(\theta)$ is relatively small.

Although the analysis thus far has been based on yearly averaged relationships of energy variables and D , the scatter plots suggest a transient effect of D over the critical depth range. A transient effect would be marked by temporal variations in the energy balances that are prompted by temporal variations of D . The time scale of the transient effect will depend on how quickly the pressure head profile adjusts to perturbations in D and is thus, influenced by the soil type, subsurface heterogeneity, vegetation cover, ambient moisture conditions, and the magnitude and duration of the perturbation. Whilst the analysis of transient effects requires additional work in future, it is obvious that large scale trends in D might cause significant changes in the energy balance at the land surface. This might be important in regions such as the Great Plains, where

large scale groundwater mining has resulted in a decline of previously shallow groundwater levels.

7.b Spatial bivariat statistics

The semivariograms of the yearly averaged water table depths (D) (Figure 12) show a strong directional dependence. The x -directional semivariogram is closely aligned with the principal flow direction of the Little Washita from west to east and therefore captures the larger scale of processes that are associated with the longitudinal river architecture. Because the y -direction is aligned normal to the principal flow direction of the Little Washita River, the scale of the D structure in the y -direction semivariogram is smaller than in the x -direction. This means the semivariogram in the y -direction mainly captures hillslope processes from the center of the valley toward the hilltops. Thus, the main process captured here is groundwater flow from recharge areas along the hillslope and hilltops toward discharge areas along the river corridor and the associated spatial variation in D .

In the analysis of cross correlations shown in Figure 13, it is important to keep in mind that nonlinearities in the dependence between water table depths and the energy variables, present in the model, are not captured by the plots. Thus, small cross correlations do not necessarily entail the absence of cross dependence. Additionally, cross correlations were calculated over the entire domain without distinguishing between vegetation and soil type. This was done to obtain an integrated measure of cross dependence at the watershed scale. On the other hand, large cross correlations do not necessarily suggest a mechanistic dependence. However, because a process-based model was used, this study is able to address this ambiguity inherent in statistical analysis.

The cross correlograms of variables with significant cross dependence exhibit distinct seasonality both in the values and in structure. This will be discussed using the ground heat flux, G , which exhibits the strongest linear cross correlation with water table depth, D .

During the summer months, G is directed from the atmosphere into the subsurface. This is shown in Figure 13 by negative cross correlations. G decreases with increasing water table depth, because drier conditions reduce the thermal conductivity of the soil, which in turn reduces G . The cross correlation reverses in September and October and remains positive during the winter months. This reversal is caused by a switch in the direction of G which is from the subsurface into the atmosphere during the winter. The positive cross correlation only indicates a reversal in the direction of G , the magnitude of G is still negatively correlated with D .

Juxtaposition of the G cross correlograms and semivariograms (Figures 13 and 14) shows that the spatial structure of G is very similar to the water table structure over most of the year. The scale of the G structure is 6 to 7km, which can be inferred from the cross correlograms and semivariograms, and is similar to the hill slope scale in the y -direction. Changes in the structure of G (Figure 14) occur when the cross correlograms are in transition from positive to negative values (March and April) or vice versa (September and October). Therefore, the change in the structure of G coincides with a change in its direction from the subsurface toward the atmosphere or vice versa. In the transition months the correlation scale decreases to about 5km and does not show directional dependence. That has implications for the design of field studies, which will be discussed below, because it demonstrates during which time periods process interactions are expected to be detectable.

The good agreement of the structure in G and D stems from their interdependence. This is reflected in the scatter plots and cross correlograms (Figure 10 and 13) and is most pronounced

when the subsurface equilibrates to the prevalent seasonal atmospheric conditions at the land surface. The scale of the G structure is shifted to slightly smaller values, mainly because of the influence of vegetation and soil cover. Additionally, hydraulic pressure perturbations from, for example, precipitation and recharge events propagating through the system on relatively small time scales also affect the spatial structure. This effect could be more pronounced for non-uniform atmospheric forcing, which is not taken into account in this study.

8. Recommendations for Future Field Studies

The simulation results suggest that PF.CLM is a useful tool in the design of field campaigns, because it affords the selection of important parameters, measurement locations and time periods. Based on the findings of this study, we recommend collecting co-located measurements of at least groundwater level, soil temperature and pressure head profiles, as well as the basic atmospheric variables. These co-located measurements should be collected at locations where the water table is in the range of the critical depth, 1-5m in this work. In cases of large ($D > 10\text{m}$) or very shallow ($D < 0.5\text{m}$) water table depths, water level measurements appear to be secondary. Figure 16 shows the scatter plot of average ground surface temperature versus water table depths at each x,y - location in the domain for the month of June 1999. For deciduous forest, croplands and open shrublands, water table depth affects ground surface temperature in the range of 2K and should be detectable from simple field measurements. For these vegetation types water table effects are on the order of land cover effects, i.e. neglecting water table effects may have the same impact as simulating open shrublands instead of croplands.

Figure 13 and 14 also suggest that cross dependence of groundwater dynamics and energy variables might only be detectable in the field for the ground heat flux, G , and ground

surface temperature. Since the cross correlations and the similarity of the spatial structure of G and D are strongest in the months when the seasonal direction of G is well established, measurement campaigns should avoid the transition months from winter to summer and vice versa. In our case, this transition occurred during March and April and September and October, respectively, though regional and yearly variations must also be taken into account

We also believe that shallow soil moisture data from the first few centimeters below the ground surface, often inferred from remote sensing data, might be inherently difficult to interpret and might not reflect the intrinsic spatial composition of the system especially under dry conditions. Soil moisture directly at the land surface does not necessarily represent the moisture availability of the underlying system. At the surface, the moisture availability and, thus, mass fluxes, are governed by the structure of the soil and the vertical gradient of the soil water pressure head throughout the soil column. Therefore the soil moisture value at the land surface does not suffice to characterize the system and is not a measure of the “true dryness” or moisture state of the system.

This point is illustrated using a simple analytical solution for steady evaporation at the ground surface for a structured soil for two different evaporation rates. Figure 17 shows depth to the water table versus relative saturation for two water table - evaporation rate (E) configurations. At the land surface and right below it, saturations for both configurations are very similar and close to the residual water content. Thus, application of Gibbs equation (Equation 5) in conjunction with boundary layer theory to calculate E will result in identical values.

However, Figure 17 shows that in case of water table A, the system is able to maintain an evaporation rate that is two times larger than in case of water table B, because of increased moisture transport toward the land surface. From this analysis, it is obvious that the saturation

value at the land surface does not allow inference of E or the “true dryness” of the subsurface if no information of $\theta(z)$ and the depth to the water table is available in the case of a homogeneous soil profile. The analysis is further complicated in the case of a heterogeneous subsurface, because knowledge of $\theta(z)$ does not suffice to infer fluxes and thus E . Knowledge of $\theta(z, \psi)$ of the material of the soil profile or direct measurements of ψ are required.

The latter also has implications for parameterizations of E in commonly applied land surface models [Mahfouf and Noilhan, 1991] that incorporate empirical resistance terms based on the shallow soil moisture profile. Knowledge of vertical soil heterogeneity and $\theta(\psi)$ relationships would be required to make the application of these parameterization schemes warranted, though this type of data is rarely available on the watershed scale.

The above analysis might also explain the spatially unstructured soil moisture patterns from remote sensing after long drying periods, because θ at the land surface is close to the residual water content and does not reflect the actual moisture fluxes. This does not mean, however, that the moisture fluxes do not show spatial patterns under dry conditions, θ simply might not be the correct indicator. We suggest humidity close to the ground surface as a better indicator for the moisture state of the system, because this parameter is directly influenced by the moisture fluxes from the subsurface.

This is illustrated in Figure 18, which shows the unit semivariograms of humidity from the Micronet stations in the Little Washita watershed. The semivariograms clearly exhibit structure with a range of about 6 to 7km, which is similar to the hillslope scale and influence by groundwater dynamics as we believe.

9. Summary and Conclusions

In this study, simulations were performed to examine the influence of groundwater dynamics on the energy and mass balance at the land surface. ParFlow, a 3D variably saturated groundwater flow model was coupled to the Common Land Model (CLM) to simulate water and energy fluxes in the subsurface and at the land surface including saturated flow in the deeper aquifer. The coupled model, PF.CLM, was applied to the Little Washita watershed, Oklahoma, USA. Continuous atmospheric time series from the North American Regional Reanalysis data set were used to force the model uniformly in space over one entire year from September 1998 to August 1999. A dynamic equilibrium, commonly referred to as spinup, was established in which the average mass and energy balance does not change over the simulation period. The simulation results were compared to measured data from a USGS stream gauging Station, an Ameriflux tower and the Soil Climate Analysis Network. The comparison showed reasonable agreement for stream discharge, latent heat and soil moisture without calibration.

The results of this study show that components of the energy balance are sensitive to groundwater dynamics, if the groundwater level is in the range of, what we define as, the critical depth that extents from 1 to 5m below the ground surface. This critical depth coincides with the root zone defined in the model. Therefore, the sensitivity of the energy variables on groundwater dynamics also depends on the land cover. Although, the connection of groundwater dynamics and surface processes clearly is a function of the parameterizations in the coupled model, we argue that the connection generally exists but can be of varying strength depending on the applied model or physical conditions.

In a second step, the spatial structure and cross dependence of the energy variables and water level was analyzed. Unit semivariograms from measured soil temperature data from Micronet stations in the Little Washita watershed agreed well with simulated semivariograms, which suggest that (1) there exists spatial structure in the energy variables and (2) the model is able to realistically capture this structure.

The underlying mechanism that generates the structure is lateral subsurface flow from recharge areas along hilltops to discharge zones along the Little Washita river corridor. Directional dependence of the structure stems from the geometry of the watershed and flow direction of the Little Washita which is predominantly in the x -direction from west to east. Semivariograms of depth to the water level and ground heat flux suggest two spatial scales of correlation, 7 and 11 km, which are the result of the aforementioned watershed geometry and the hillslope scale. Structure in the ground heat flux is predominantly determined by the underlying water table structure, but deteriorates during the transition from warm to cold months and vice versa.

Spatial cross dependence derived from cross correlograms is significant only in the case of ground heat flux, ground surface temperature and possibly latent heat. Cross dependence exists on a scale similar to the hillslope scale, which suggests lateral subsurface flow toward the Little Washita River as the underlying mechanism.

This study calls attention to the need for co-located measurements of groundwater level, soil pressure head, soil temperature and standard atmospheric variables, which are virtually non-existent. These co-located measurements are needed in spatially distributed fashion to identify the interconnection of groundwater dynamics and the mass and energy balance at the land surface as well as any spatial structure and cross dependence that potentially exists. This study

also points to the usefulness of the applied coupled model in process identification, measurement network design and data analysis.

A deeper analysis of shallow soil moisture using a simple analytical solution for steady evaporation reveals the limited information content of this variable about the moisture state of the system in the case of shallow groundwater. This should be taken into consideration in studies related to the interactions of the land surface and the lower atmospheric boundary layer. Finally, the model is useful in providing realistic soil moisture initial conditions for atmospheric models that do not account for groundwater dynamics [Maxwell, *et al.*, 2007].

10. Acknowledgements.

This work was conducted under the auspices of the U. S. Department of Energy by the University of California, Lawrence Livermore National Laboratory (LLNL) under contract W-7405-Eng and was supported by the LLNL Laboratory Directed Research and Development Program at LLNL and by DOE Fossil Energy Program NETL, NPTO, Tulsa, OK. This work may be cited using UCRL-TR-228343.

11. References

- Alley, W. M., R. W. Healy, J. W. LaBaugh, and T. E. Reilly (2002), Hydrology - Flow and storage in groundwater systems, *Science*, 296, 1985-1990.
- Ashby, S. F., and R. D. Falgout (1996), A parallel multigrid preconditioned conjugate gradient algorithm for groundwater flow simulations, *Nucl Sci Eng*, 124, 145-159.
- Betts, A. K., J. H. Ball, A. C. M. Beljaars, M. J. Miller, and P. A. Viterbo (1996), The land surface-atmosphere interaction: A review based on observational and global modeling perspectives, *J Geophys Res-Atmos*, 101, 7209-7225.

Chen, T. H., A. HendersonSellers, P. C. D. Milly, A. J. Pitman, A. C. M. Beljaars, J. Polcher, F. Abramopoulos, A. Boone, S. Chang, F. Chen, Y. Dai, C. E. Desborough, R. E. Dickinson, L. Dumenil, M. Ek, J. R. Garratt, N. Gedney, Y. M. Gusev, J. Kim, R. Koster, E. A. Kowalczyk, K. Laval, J. Lean, D. Lettenmaier, X. Liang, J. F. Mahfouf, H. T. Mengelkamp, K. Mitchell, O. N. Nasonova, J. Noilhan, A. Robock, C. Rosenzweig, J. Schaake, C. A. Schlosser, J. P. Schulz, Y. Shao, A. B. Shmakin, D. L. Verseghy, P. Wetzell, E. F. Wood, Y. Xue, Z. L. Yang, and Q. Zeng (1997), Cabauw experimental results from the project for intercomparison of land-surface parameterization schemes, *J Climate*, 10, 1194-1215.

Chen, X., and Q. Hu (2004), Groundwater influences on soil moisture and surface evaporation, *J Hydrol*, 297, 285-300.

Chow, F. K., A. P. Weigel, R. L. Street, M. W. Rotach, and M. Xue (2006), High-resolution large-eddy simulations of flow in a steep Alpine valley. Part I: Methodology, verification, and sensitivity experiments, *J Appl Meteorol Clim*, 45, 63-86.

Dai, X. P., X. Zeng, and C. D. Dickinson (2001), The Common Land Model (CLM): Technical documentation and user's guide.

Dai, Y. J., X. B. Zeng, R. E. Dickinson, I. Baker, G. B. Bonan, M. G. Bosilovich, A. S. Denning, P. A. Dirmeyer, P. R. Houser, G. Y. Niu, K. W. Oleson, C. A. Schlosser, and Z. L. Yang (2003), The Common Land Model, *B Am Meteorol Soc*, 84, 1013-+.

Grayson, R. B., G. Bloschl, A. W. Western, and T. A. McMahon (2002), Advances in the use of observed spatial patterns of catchment hydrological response, *Adv Water Resour*, 25, 1313-1334.

- Henderson-Sellers, A., and B. Henderson-Sellers (1995), Simulating the diurnal temperature range: Results from phase 1(a) of the project for intercomparison of landsurface parameterisation schemes (PILPS), *Atmos Res*, 37, 19.
- Holt, T. R., D. Niyogi, F. Chen, K. Manning, M. A. LeMone, and A. Qureshi (2006), Effect of land-atmosphere interactions on the IHOP 24-25 May 2002 convection case, *Mon Weather Rev*, 134, 113-133.
- Jackson, J. E., D. M. L. Vine, A. Y. Hsu, A. Oldak, P. Starks, C. T. Swift, J. D. Isham, and M. Haken (1999), Soil moisture mapping at regional scale using microwave radiometry: The Southern Great Plains Hydrology Experiment, *Ieee T Geosci Remote*, 37, 15.
- Jones, J. E., and C. S. Woodward (2001), Newton-Krylov-multigrid solvers for large-scale, highly heterogeneous, variably saturated flow problems, *Adv Water Resour*, 24, 763-774.
- Kollet, S. J., and R. M. Maxwell (2006), Integrated surface-groundwater flow modeling: A free-surface overland flow boundary condition in a parallel groundwater flow model, *Adv Water Resour*, 29, 945-958.
- Liang, X., Z. H. Xie, and M. Y. Huang (2003), A new parameterization for surface and groundwater interactions and its impact on water budgets with the variable infiltration capacity (VIC) land surface model, *J Geophys Res-Atmos*, 108, -.
- Lohmann, D., D. P. Lettenmaier, X. Liang, E. F. Wood, A. Boone, S. Chang, F. Chen, Y. J. Dai, C. Desborough, R. E. Dickinson, Q. Y. Duan, M. Ek, Y. M. Gusev, F. Habets, P. Irannejad, R. Koster, K. E. Mitchell, O. N. Nasonova, J. Noilhan, J. Schaake, A. Schlosser, Y. P. Shao, A. B. Shmakin, D. Verseghy, K. Warrach, P. Wetzels, Y. K. Xue, Z. L. Yang, and Q. C. Zeng (1998), The Project for Intercomparison of Land-surface

- Parameterization Schemes (PILPS) phase 2(c) Red-Arkansas River basin experiment: 3. Spatial and temporal analysis of water fluxes, *Global Planet Change*, 19, 161-179.
- Mahfouf, J. F., and J. Noilhan (1991), Comparative-Study of Various Formulations of Evaporation from Bare Soil Using Insitu Data, *J Appl Meteorol*, 30, 1354-1365.
- Manabe, S., Smagorin.J, J. L. Holloway, and H. M. Stone (1970), Simulated Climatology of a General Circulation Model with a Hydrologic Cycle, *Mon Weather Rev*, 98, 175-&.
- Maxwell, R. M., F. K. Chow, and S. J. Kollet (2007), Effects of groundwater storage and surface and subsurface lateral flow on the atmospheric boundary layer in a coupled groundwater, land-surface, and mesoscale atmospheric model, *Adv Water Resour*, (in review).
- Maxwell, R. M., and N. L. Miller (2005), Development of a coupled land surface and groundwater model, *J Hydrometeorol*, 6, 233-247.
- NRC, N. R. C. (2004), Groundwater fluxes across interfaces, *The National Academic Press, Washington, D.C.*, 85.
- Patton, E. G., P. P. Sullivan, and C. H. Moeng (2005), The influence of idealized heterogeneity on wet and dry planetary boundary layers coupled to the land surface, *J Atmos Sci*, 62, 2078-2097.
- Pitman, A. J., A. Henderson-Sellers, C. E. Desborough, Z. L. Yang, F. Abramopoulos, A. Boone, R. E. Dickinson, N. Gedney, R. Koster, E. Kowalczyk, D. Lettenmaier, X. Liang, J. F. Mahfouf, J. Noilhan, J. Polcher, W. Qu, A. Robock, C. Rosenzweig, C. A. Schlosser, A. B. Shmakin, J. Smith, M. Suarez, D. Verseghy, P. Wetzel, E. Wood, and Y. Xue (1999), Key results and implications from phase 1(c) of the Project for Intercomparison of Land-Surface Parametrization Schemes, *Clim Dynam*, 15, 673-684.

- Qu, W. Q., A. Henderson-Sellers, A. J. Pitman, T. H. Chen, F. Abramopoulos, A. Boone, S. Chang, F. Chen, Y. Dai, R. E. Dickinson, L. Dumenil, M. Ek, N. Gedney, Y. M. Gusev, J. Kim, R. Koster, E. A. Kowalczyk, J. Lean, D. Lettenmaier, X. Liang, J. F. Mahfouf, H. T. Mengelkamp, K. Mitchell, O. N. Nasonova, J. Noilhan, A. Robock, C. Rosenzweig, J. Schaake, C. A. Schlosser, J. P. Schulz, A. B. Shmakin, D. L. Verseghy, P. Wetzel, E. F. Wood, Z. L. Yang, and Q. Zeng (1998), Sensitivity of latent heat flux from PILPS land-surface schemes to perturbations of surface air temperature, *J Atmos Sci*, 55, 1909-1927.
- Quinn, P., K. Beven, and A. Culf (1995), The Introduction of Macroscale Hydrological Complexity into Land Surface-Atmosphere Transfer Models and the Effect on Planetary Boundary-Layer Development, *J Hydrol*, 166, 421-444.
- Schaap, M. G., and F. J. Leij (1998), Database-related accuracy and uncertainty of pedotransfer functions, *Soil Sci*, 163, 765-779.
- Schlosser, C. A., A. G. Slater, A. Robock, A. J. Pitman, K. Y. Vinnikov, A. Henderson-Sellers, N. A. Speranskaya, K. Mitchell, P. D. Contributors, and (2000), Simulations of a boreal grassland hydrology at Valdai, Russia: PILPS phase 2(D), *Mon Weather Rev*, 128, 301-321.
- Shao, Y. P., and A. HendersonSellers (1996), Modeling soil moisture: A project for intercomparison of land surface parameterization schemes phase 2(b), *J Geophys Res-Atmos*, 101, 7227-7250.
- Sophocleous, M., and S. P. Perkins (2000), Methodology and application of combined watershed and ground-water models in Kansas, *J Hydrol*, 236, 185-201.

- Sophocleous, M. A., J. K. Koelliker, R. S. Govindaraju, T. Birdie, S. R. Ramireddygari, and S. P. Perkins (1999), Integrated numerical modeling for basin-wide water management: The case of the Rattlesnake Creek basin in south-central Kansas, *J Hydrol*, 214, 179-196.
- Toth, J. (1963), A Theoretical Analysis of Groundwater Flow in Small Drainage Basins, *J Geophys Res*, 68, 4795-&.
- Twine, T. E., W. P. Kustas, J. M. Norman, D. R. Cook, P. R. Houser, T. P. Meyers, J. H. Prueger, P. J. Starks, and M. L. Wesely (2000), Correcting eddy-covariance flux underestimates over a grassland, *Agr Forest Meteorol*, 103, 279-300.
- Yeh, P. J. F., and E. A. B. Eltahir (2005), Representation of water table dynamics in a land surface scheme. Part I: Model development, *J Climate*, 18, 1861-1880.
- York, J. P., M. Person, W. J. Gutowski, and T. C. Winter (2002), Putting aquifers into atmospheric simulation models: an example from the Mill Creek Watershed, northeastern Kansas, *Adv Water Resour*, 25, 221-238.

Figure Captions

Figure 1. Schematic of the interconnection between groundwater (GW), shallow soil moisture (SM) and land surface (LS) processes: shallow groundwater (Case 1); groundwater at intermediate aquifer depth (Case 2); and deep groundwater (Case 3).

Figure 2. Schematic cross-section of the land surface and the water table showing theoretical delineation of three zones of influence of groundwater on land surface processes as a function of groundwater depth.

Figure 3. Location of the Little Washita watershed. The inset shows the location of the watershed in the state of Oklahoma. The footprint of the DOE ARM site is shown in the inset.

Figure 4. Plot of relative soil saturation, S , for the entire Little Washita watershed model for mid June, 1999. Note the watershed outline from Figure 3 is overlain on the land surface.

Figure 5. Spatially distributed soil (left) and vegetation cover (right) information used in the simulations.

Figure 6. Comparison of the simulated and measured hydrograph from the USGS gauging station 7327550.

Figure 7. Comparison of simulated and measured soil moisture from the SCAN site.

Figure 8. Comparison of simulated daily averaged latent heat with the data from the Ameriflux tower.

Figure 9. Plots of yearly-averaged a) topography; b) depth to water table c) relative soil saturation; d) ground surface temperature; e) net radiation; f) latent heat flux; g) sensible heat flux; and h) ground heat flux.

Figure 10. Semi-logarithmic scatter plots of yearly averaged a) net radiation; b) latent heat; c) sensible heat; and d) ground heat flux as a function of water table depth. The gray areas indicate the root zone depth. The dashed lines separate three segments that characterize the curves for different vegetation types. Note the different scales for the y-axes in this Figure.

Figure 11. Unit variograms for shallow soil temperature from the simulation and Micronet monitoring network in the Little Washita watershed.

Figure 12. Semivariograms in the x and y direction for yearly averaged water table depths values.

Figure 13. Cross correlations of the components of the energy balance and ground surface temperature with water table depth (R_n , net radiation; LE, latent heat; H, sensible heat; G, ground heat flux; T_s , ground surface temperature).

Figure 14. Directional semivariograms for ground heat flux, G , and water table depth, D , for each month of the year.

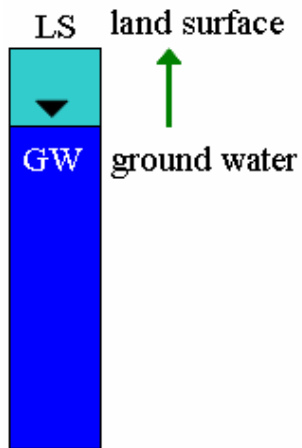
Figure 15. Semi logarithmic plot of relative humidity, h_r , and relative saturation, S_E , versus soil pressure head as predicted by Gibbs' and vanGenuchten formulae. A wilting point value of 150m suction is indicated with the dotted line. Note that pressure head is always negative (in suction) in this plot.

Figure 16. Scatter plot of average ground surface temperature versus water table depth for the month of June 1999. The depth of the root zone is indicated with the gray area.

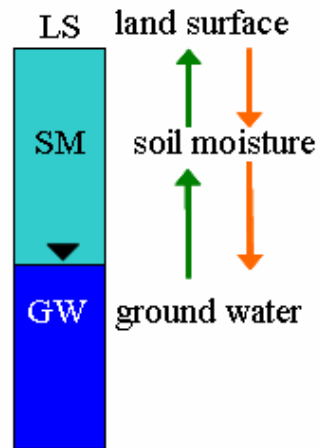
Figure 17. Depth below ground surface for two evaporation rate – water table configurations. Water table A corresponds to evaporation rate $E = 0.035$ mm/h and water table B corresponds to $E = 0.07$ mm/h.

Figure 18. Unit variograms for air humidity from the Micronet monitoring network in the Little Washita watershed.

Shallow groundwater



Groundwater at critical depth



Deep groundwater

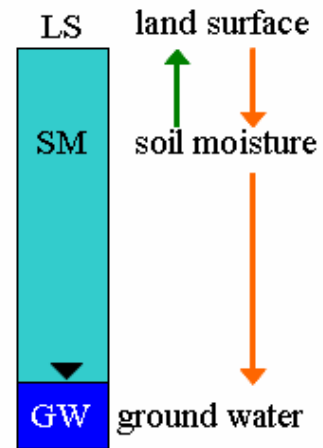


Figure 1.

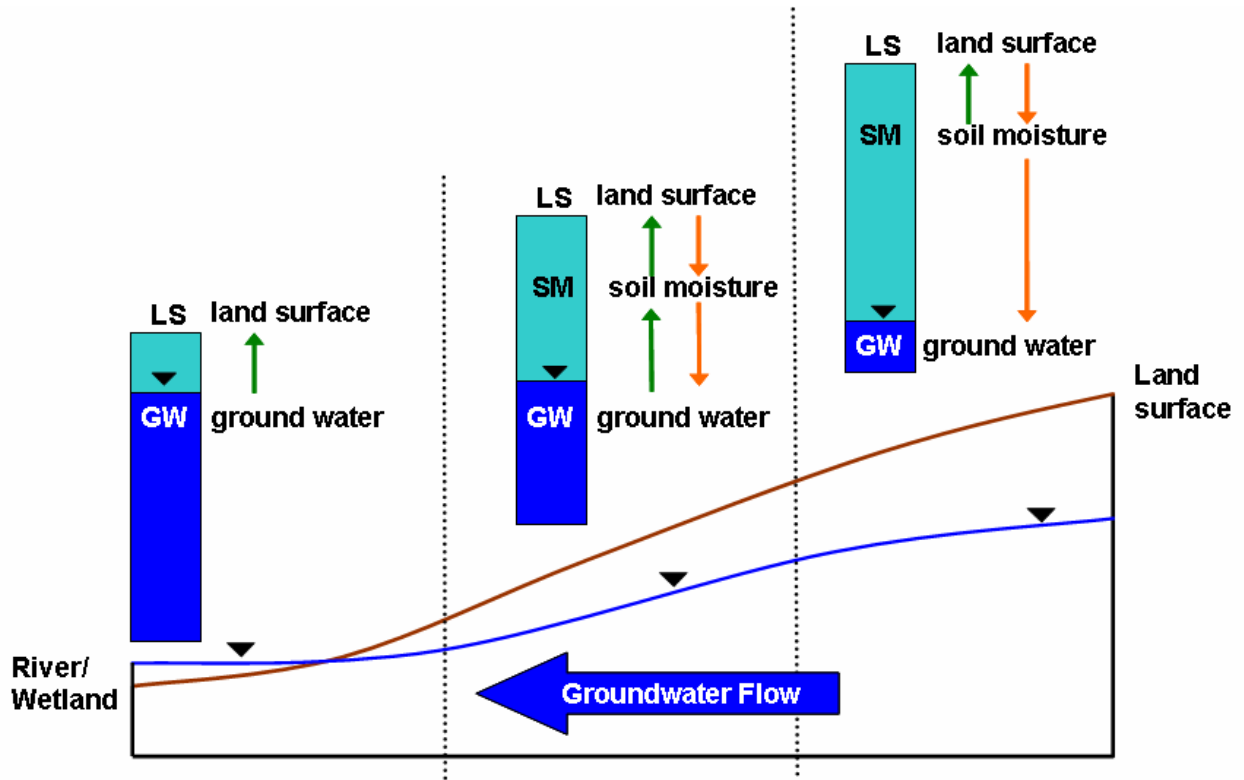


Figure 2.

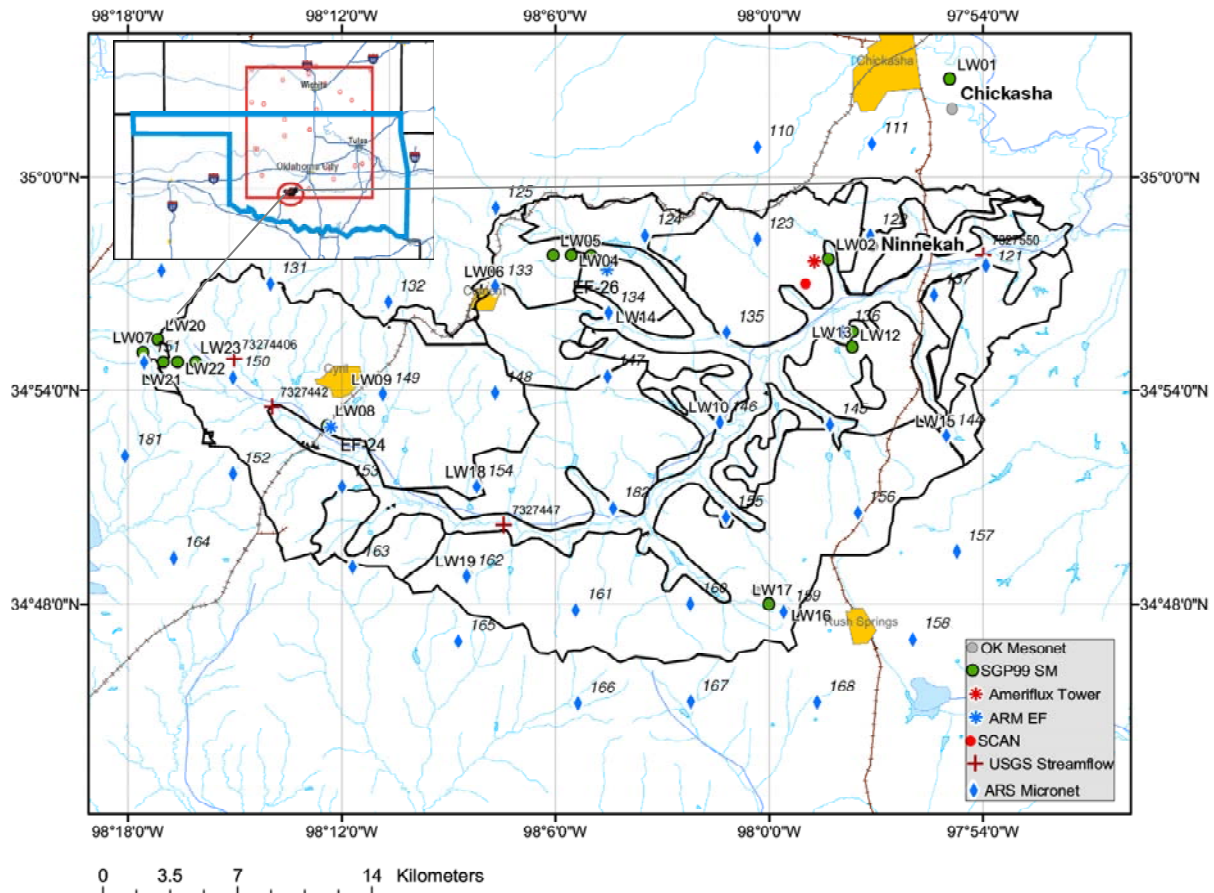


Figure 3.

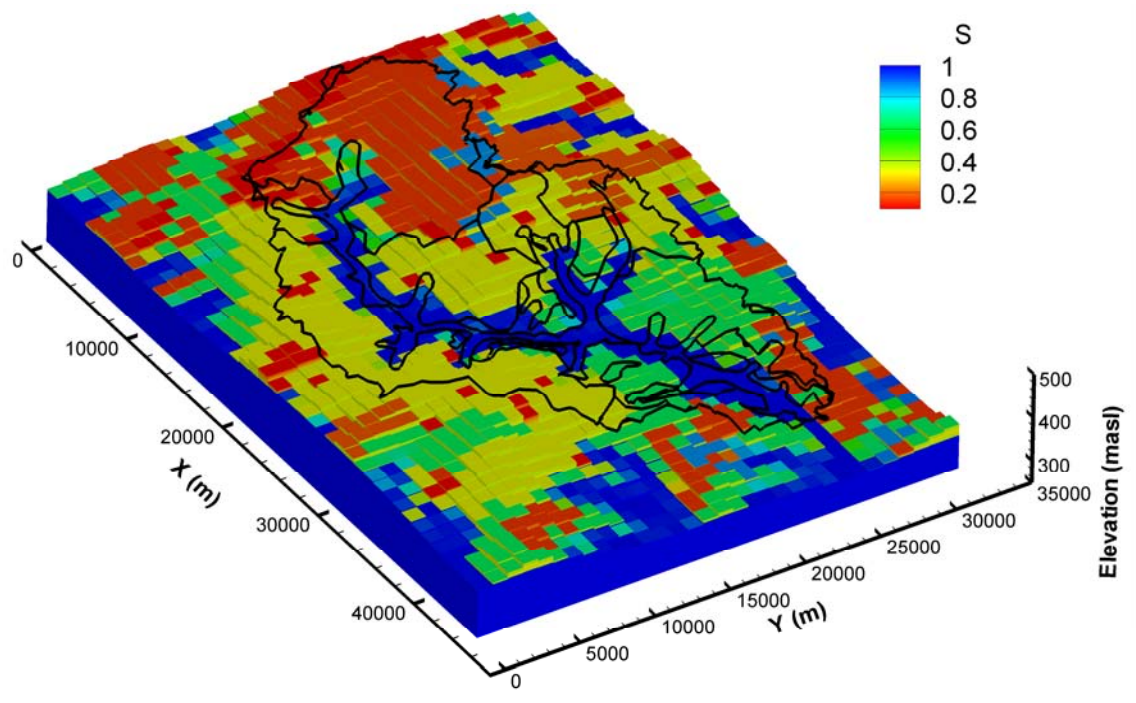


Figure 4.

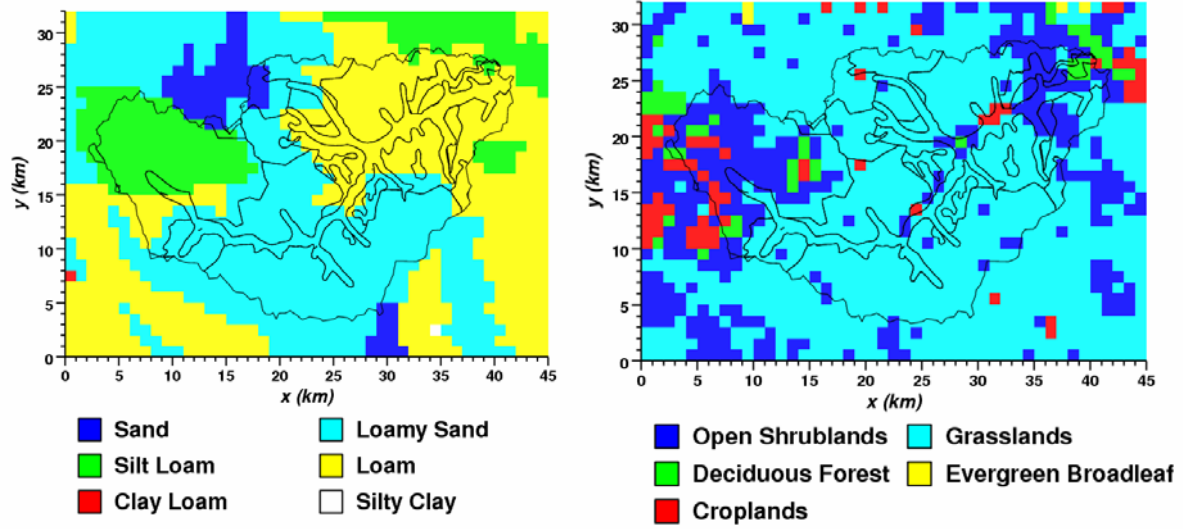


Figure 5.

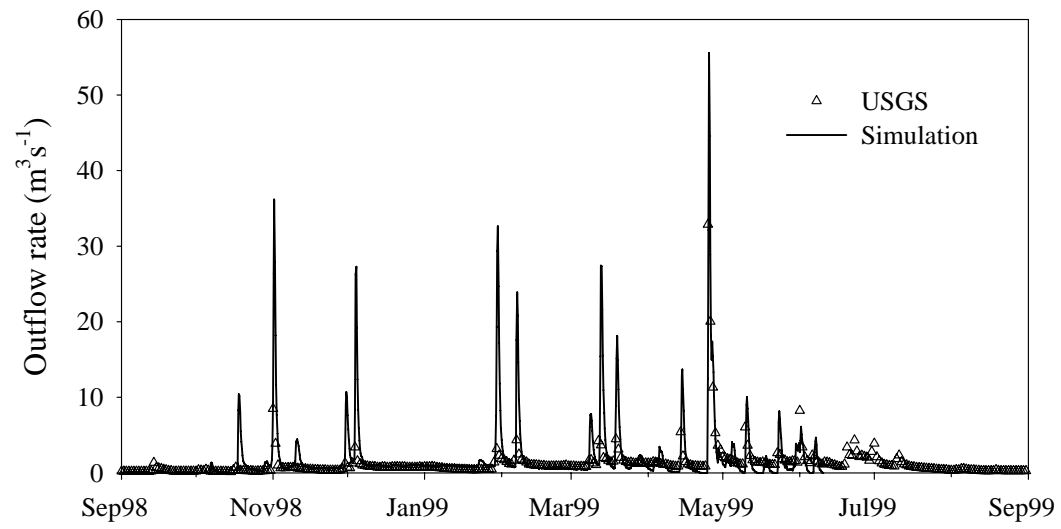


Figure 6.

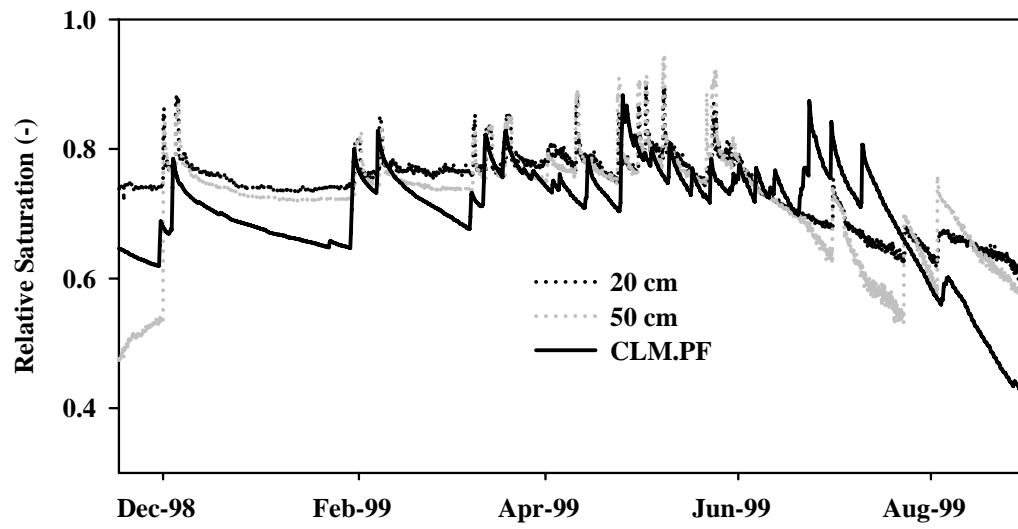


Figure 7.

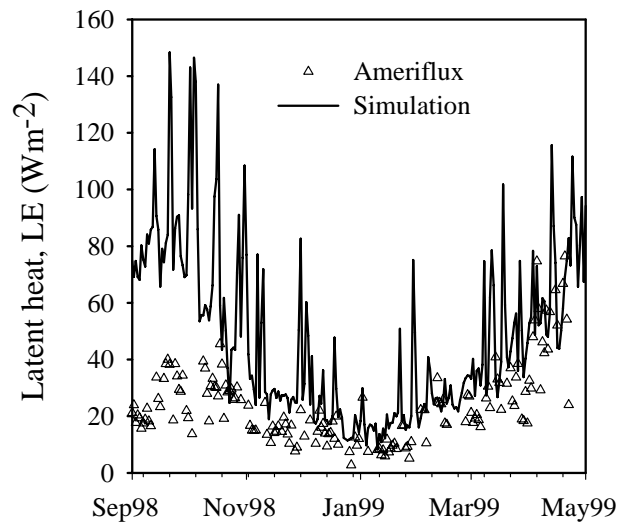


Figure 8.

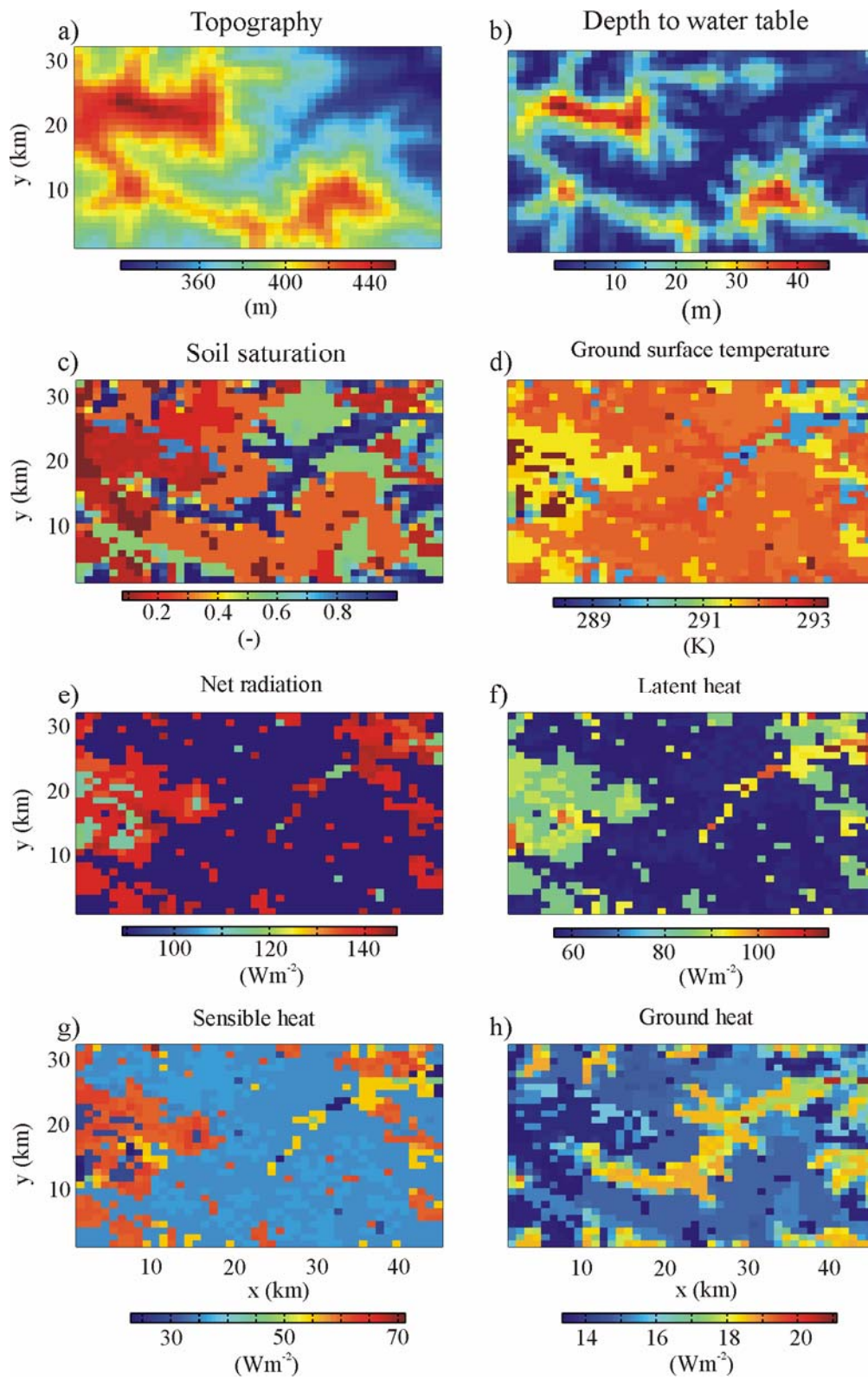


Figure 9.

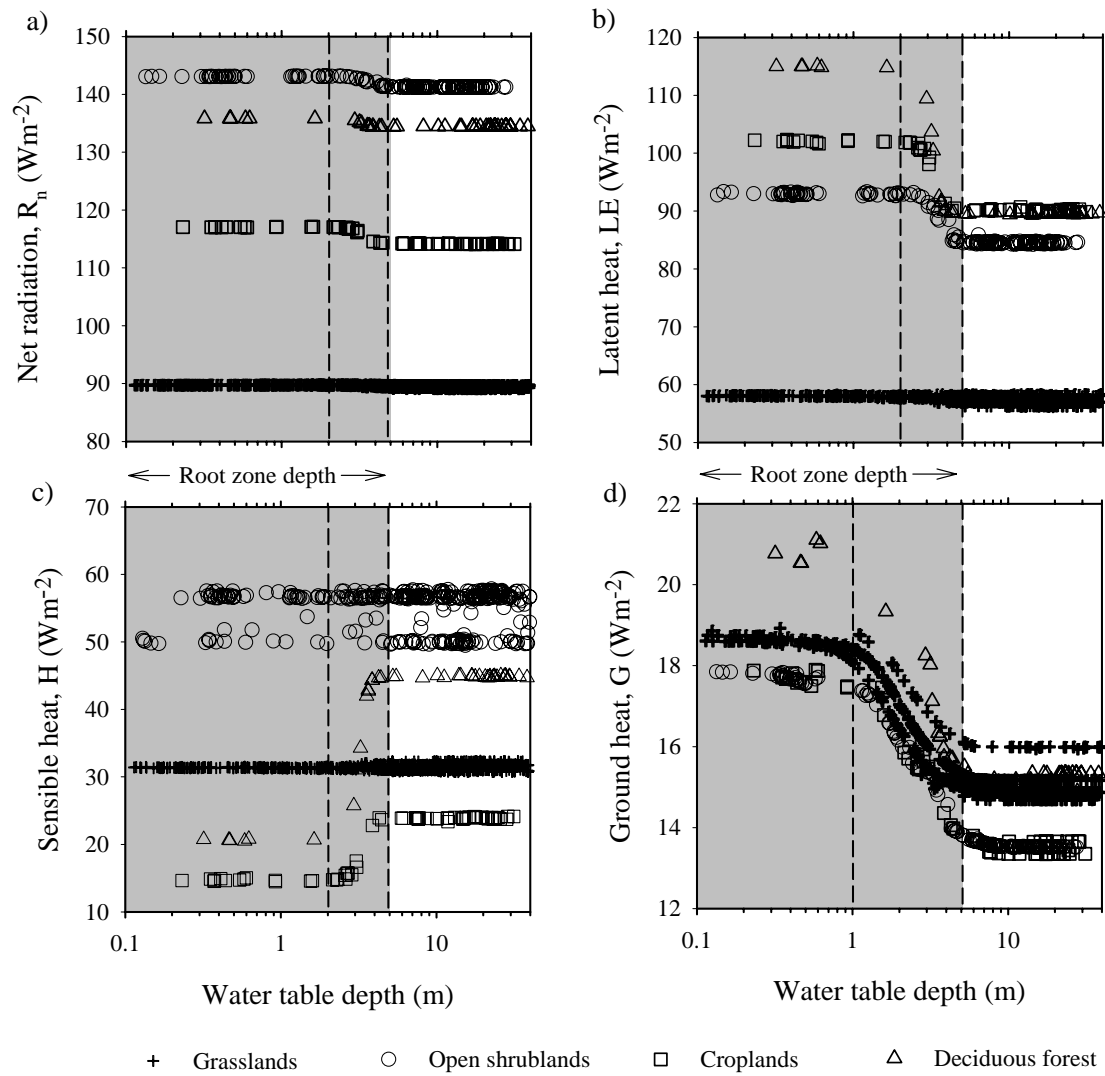


Figure 10.

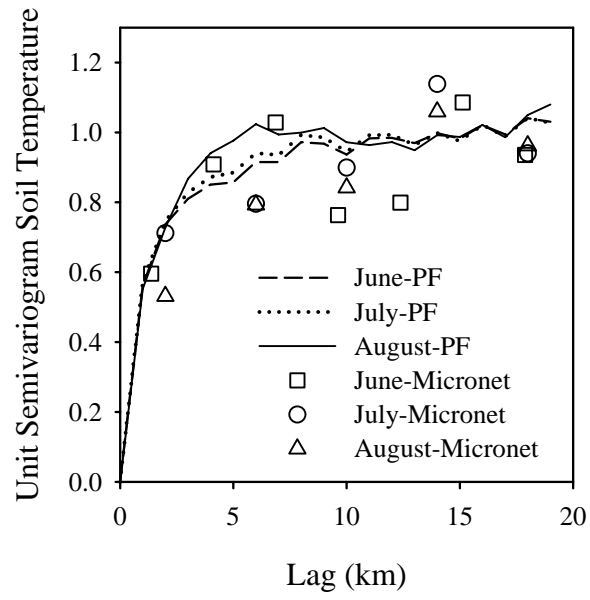


Figure 11.

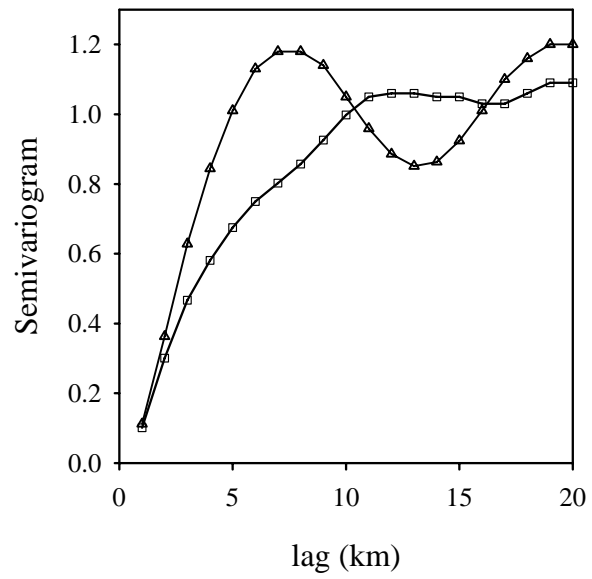


Figure 12.

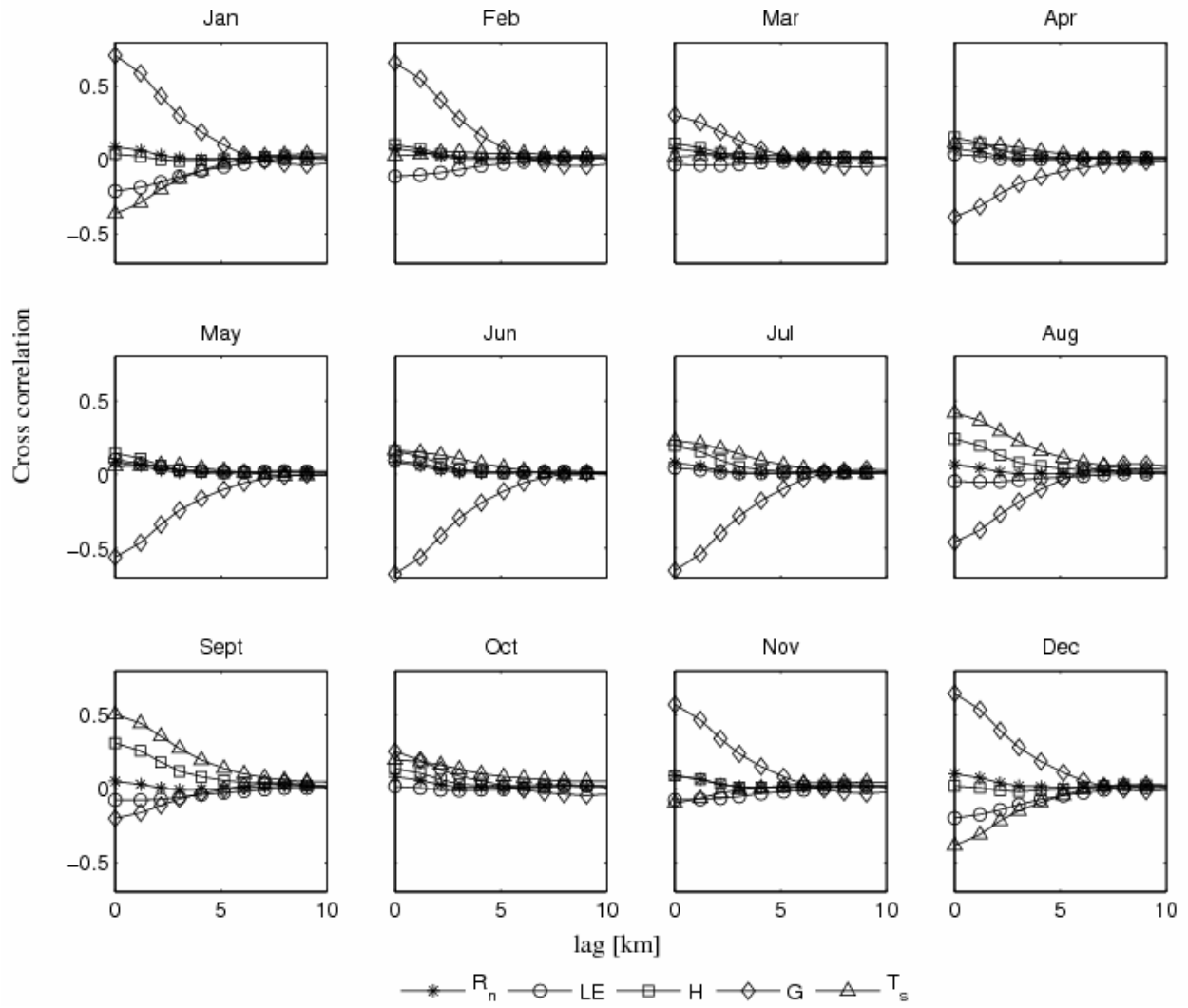


Figure 13.

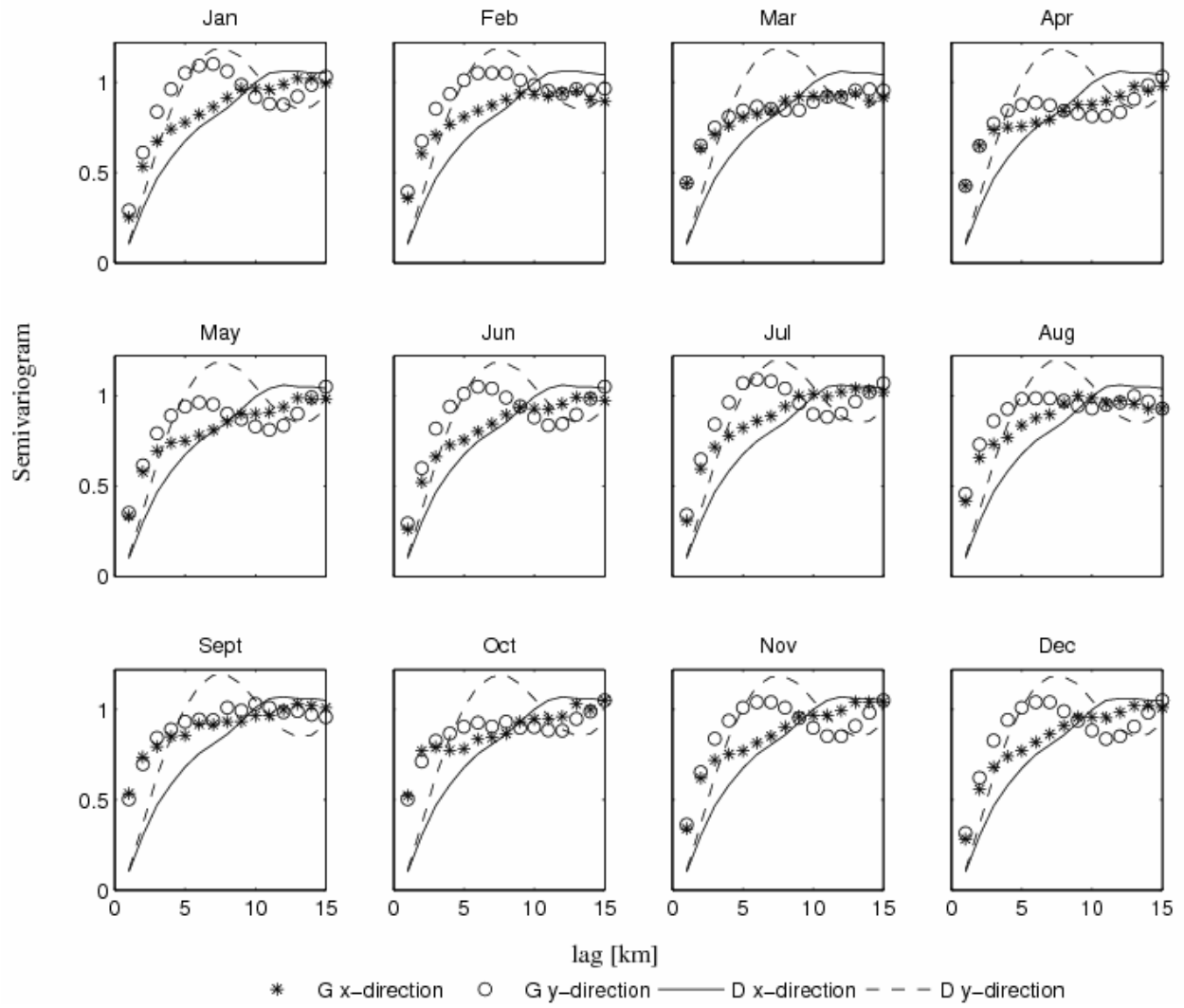


Figure 14.

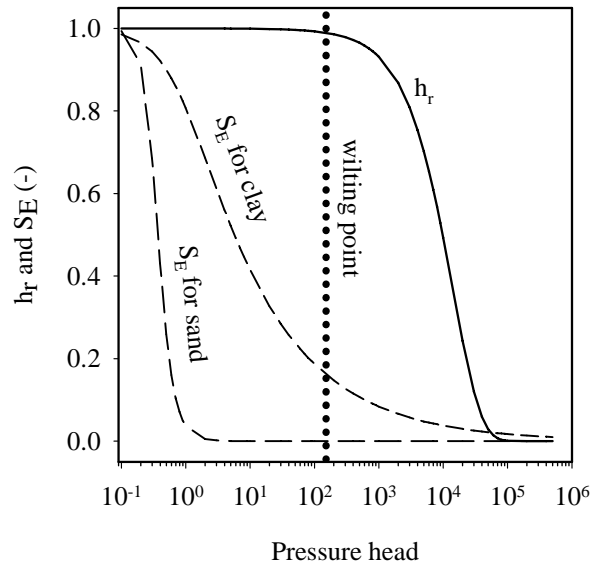


Figure 15.

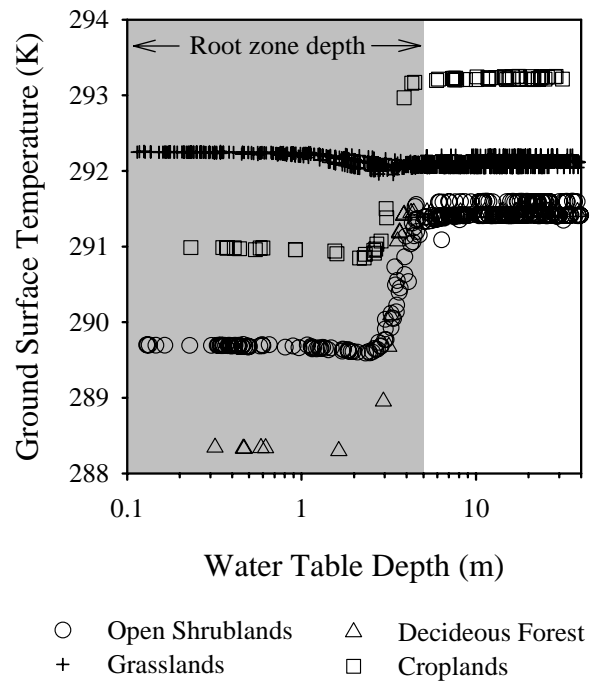


Figure 16.

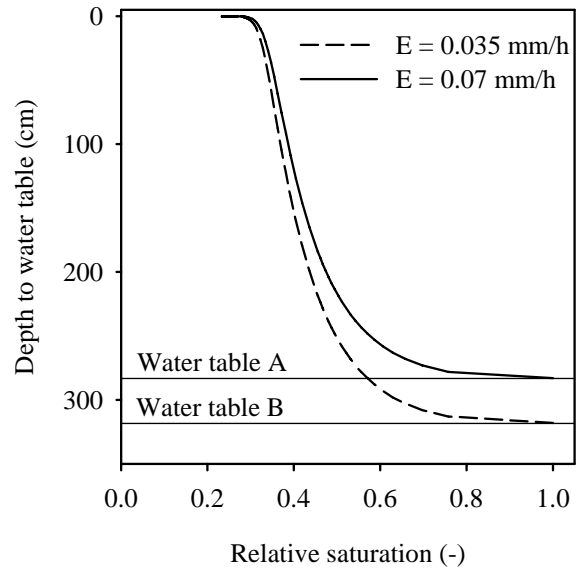


Figure 17.

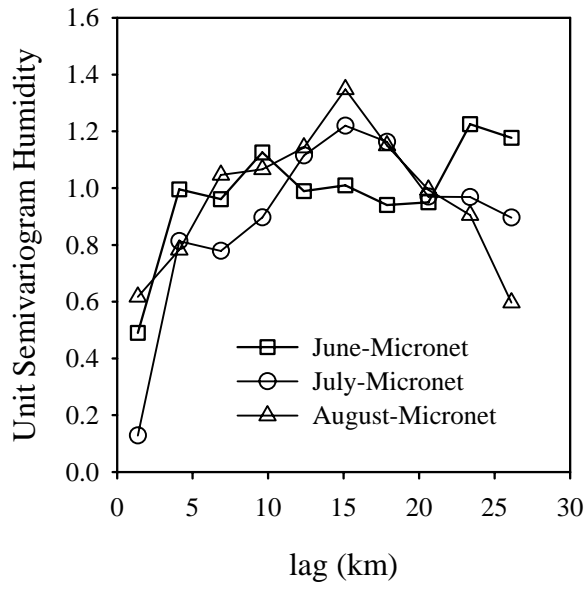


Figure 18.